# Integrated Frequency-constrained Scheduling Considering Coordination of Frequency Regulation Capabilities from Multi-source Converters

Jiaming Li, Ying Qiao, Zongxiang Lu, Wei Ma, Xin Cao, and Rongfu Sun

***Abstract*—As the proportion of renewable energy (RE) increases, the inertia and the primary frequency regulation (FR) capability of the power system decrease. Thus, ensuring frequency security in the scheduling model has become a new technical requirement in power systems with a high share of RE. Due to a shortage of conventional synchronous generators, the frequency support of multi-source converters has become an indispensable part of the system frequency resources, especially variable-speed wind turbine generation (WTG) and battery energy storage (BES). Quantitative expression of the FR capability of multi-source converters is necessary to construct frequency-constrained scheduling model. However, the frequency support performance of these converter-interfaced devices is related to their working states, operation modes, and parameters, and the complex coupling of these factors has not been fully exploited in existing models. In this study, we propose an integrated frequency-constrained scheduling model considering the coordination of FR capabilities from multi-source converters. Switchable FR control strategies and variable FR parameters for WTG with or without reserved power are modeled, and multi-target allocation of BES capacity between tracking dispatch instruction and emergency FR is analyzed. Then, the variable FR capabilities of WTG and BES are embedded into the integrated frequency-constrained scheduling model. The nonlinear constraints for frequency security are precisely linearized through an improved iteration-based strategy. The effectiveness of the proposed model is verified in a modified IEEE 24-bus standard system. The results suggest that the coordinated participation of BES and WTG in FR can effectively reduce the cost of the scheduling model while meeting frequency security constraints.**

***Index Terms*—Battery energy storage (BES), wind turbine generation (WTG), frequency regulation (FR), frequency security, power system scheduling.**

Manuscript received: November 1, 2022; revised: January 10, 2023; accepted: March 9, 2023. Date of CrossCheck: March 9, 2023. Date of online publication: May 25, 2023.

This work was supported by the National Key Research and Development Program of China (No. 2021YFB2400500) and the Science and Technology Project of State Grid Corporation of China "Fast control of photovoltaic and wind power plant for transient frequency/voltage support".



J. Li, Y. Qiao, Z. Lu (corresponding author), and W. Ma are with the Department of Electrical Engineering, Tsinghua University, Beijing 100084, China (e-mail: jm-li19@mails. tsinghua. edu. cn; qiaoying@tsinghua. edu. cn; luzongxiang98@tsinghua.edu.cn; 2437331975@qq.com).

X. Cao is with the China Suntien Green Energy Limited Company, Shijiazhuang 050011, China (e-mail: caoxin@suntien.com).

R. Sun is with the State Grid Jibei Electric Power Company, Beijing 100054, China (e-mail: hcxsrf@163.com).

DOI: 10.35833/MPCE.2022.000717

## NOMENCLATURE

### A. Indices and Sets

| | |
|---|---|
| $\Omega_n^G, \Omega_n^W, \Omega_n^{PV}, \Omega_n^B$ | Sets of synchronous generators (SGs), wind farms, photovoltaic (PV) plants, and battery energy storage (BES) connected at bus $n$ |
| $\Omega_n^{LS}, \Omega_n^{LE}$ | Sets of transmission lines starting from and ending at bus $n$ |
| $b$ | Index of BESs from 1 to $N_B$ |
| $g$ | Index of SGs from 1 to $N_G$ |
| $i$ | Index of renewable energy (RE) scenarios from 1 to $N_I$ |
| $l$ | Index of transmission lines from 1 to $N_L$ |
| $m$ | Index of subspaces from 1 to $M$ |
| $n$ | Index of bus nodes from 1 to $N_N$ |
| $p$ | Index of scheduling periods from 1 to $N_P$ |
| $pv$ | Index of PV |
| $t$ | Time after contingency |
| $w$ | Index of wind turbine generation (WTG) |
| (+), (–) | Indices of start and end of a line |

### B. Parameters

| | |
|---|---|
| $\eta_b^{ch}, \eta_b^{dis}$ | Charging and discharging efficiencies of BES |
| $\Lambda$ | Discriminant of differential equations |
| $\xi$ | Coefficient of correction for output power of WTG |
| $\pi$ | Fitting parameters of $L^{\chi}$ |
| $\chi, \underline{\chi}$ | The maximum allowable imbalanced power under frequency nadir constraints and its lower bound |
| $\Gamma$ | Domain of definition of $\chi$ |
| $\omega_{\max}, \omega_{\min}$ | The maximum and minimum rotor speeds of WTG |
| $C_1, C_2, D_1, D_2, \alpha, \Omega, A, \varphi$ | Intermediate parameters of frequency dynamic equations |
| $C_b^{dis}, C_b^{ch}$ | Discharging and charging costs of BES |
| $C_g^{su}, C_g^{sd}, C_g^{nl}, C_g^{gen}$ | Start-up, shut-down, no-load, and variable costs of SG |
| $C_l$ | Penalty cost of load shedding |

$f_0$ Rated frequency

$|f_{nadir,set}|$, $|\Delta f_{nadir,set}|$ The minimum frequency nadir and the maximum acceptable frequency deviation for security

$|f_{ss,set}|$ The minimum steady-state frequency for security

$H_g, K_g$ Inertia and droop constants of individual SG

$H_{rated}^{PURM}$ Rated virtual inertial constant of WTG in power unreserved mode (PURM)

$K^L$ Droop coefficient of load

$L^\chi$ Linear equations approximating $\chi$

$L_{l,\max}$, $\theta_{\max}$ The maximum power flow of transmission line and voltage angle of bus

$P_b^{B,\max}, E_b^{B,\max}$ The maximum installed power and capacity of BES

$P_g^{G,\min}, P_g^{G,\max}$ The minimum and maximum output power of SG

$P^L, P^W, P^{PV}$ Forecasting load, WTG power, and PV power

$Pr$ Probability of each RE scenario

$P_{IM}$ Imbalanced power of contingency

$R_b^B$ Hourly ramp capacity of BES

$|ROCOF_{\max,set}|$ The maximum rate of change of frequency (ROCOF) for security

$ROCOF_{threshold}$ ROCOF threshold to trigger BES emergency frequency support mode

$R_g^{up}$, $R_g^{dn}$ Hourly ramp-up and ramp-down capacities of SG

$r_L, r_{RE}$ Forecasting errors of load and RE

$SOC_b^{\min}$, $SOC_b^{\max}$ Lower and upper limits of state of charge (SOC)

$S_g$ Rated capacity of individual SG

$S_{sys}$ Rated capacity of system

$S_w$ Installed capacity of WTG

$T_b^{ir}, T_b^{pfr}, T_b^{end}$ Time points of BES providing frequency regulation (FR)

$T_g^{on}, T_g^{off}$ The minimum on and off time of SG

$T^G$ Constant time of SG speeder

$t_{nadir}$ The time when frequency nadir occurs

$x_l$ Reactance of transmission line

### C. Variables

$\beta_w$ Proportion of WTG in power reserved mode (PRM)

$\Delta P_w^{PRM}, \Delta P_w^{PURM}$ Power increase of WTG under PRM and PURM

$\theta$ Voltage angle of bus

$\omega$ Rotor speed of WTG

$C_{sys}$ Total cost of system

$E_b^B, E_b^{B,f}$ Remaining and reserved capacities of BES

$f, \Delta f$ System frequency and frequency deviation

$f_{nadir}, f_{ss}$ Frequency nadir and steady-state frequency

$H^G, K^G$ Inertia and droop coefficient of aggregated SG

$H^{SYS}, \underline{H}^{SYS}$ Inertia of system and its lower bound

$H^{PRM}, H^{PURM}$ Virtual inertia of WTG under PRM and PURM

$K^{PRM}$ Droop constant of WTG under PRM

$K^{SYS}$ Summation of droop coefficients of load and WTG

$K^{SS}$ Summation of droop coefficients of load, WTG, and SG

$L_l$ Power flow of transmission line

$P_b^B$ Output power of BES

$P_b^{B,ch}, P_b^{B,dis}$ Charging and discharging power of BES

$P_b^{B,end}$ Power of BES at the end of FR

$P^G$ Power of SG

$P^{L,loss}$ Load shedding power

$P_{MPPT}$ The maximum power point tracking (MPPT) power of WTG

$P_{IM}^{SYS}, P_{IM}^{SYS,end}$ Equivalent imbalanced power of system at the start and end of FR

$P^{W,loss}, P^{PV,loss}$ Power of wind and PV curtailments

$R_w^W$ Total reserved wind power

$R_w^{W,H}, R_w^{W,K}$ Reserved wind power for inertia and droop supports

$u_b^{ch}, u_b^{dis}$ Charging and discharging states of BES

$u_{g,p}^{su}, u_{g,p}^{sd}, u_{g,p}$ Start-up, shut-down, and on-off states of SG

## I. Introduction

RENEWABLE energy (RE) generation have developed rapidly in recent years [1], [2]. Wind turbine generation (WTG) and photovoltaic (PV) plants are connected to the power system through power electronic interfaces, and their output power decouples with system frequency [3] in the maximum power point tracking (MPPT) mode. Both the natural inertia and the primary frequency regulation (FR) capability of the system decrease with the growing proportion of RE. Traditionally, the scheduling models such as day-ahead unit commitment (UC) and intraday economic dispatch (ED) place the greatest importance on steady-state power and electricity balances. The inertia and primary FR capability of the system are adequate to ensure frequency security because there are usually enough online synchronous generators (SGs). However, in a power system with a high share of RE, the FR capability diminishes due to the reduction of online SGs. The rate of change of frequency (ROCOF), frequency nadir, and steady-state frequency of the power grid may violate the security boundaries under frequency contingency, causing under-frequency load shedding. Only ensuring the steady-state power and electricity balances cannot guarantee sufficient system inertia, so the consideration of frequency dynamics in the timescale of UC and ED has become a new technical requirement [4]-[9]. The frequency dynamic indices are expressed as functions of the system operation states and added to the traditional scheduling model as constraints. Using frequency-constrained scheduling, more SGs and other system reserves can be arranged online to provide the required frequency support.

In addition to SGs, FR can also be provided by converter-

based equipment such as WTG [10] and battery energy storage (BES) equipment [11]. With the increase of converter-based equipment, the frequency support from converters cannot be ignored. SGs and multi-source converters together constitute system FR resources. However, the FR capabilities of converters are highly related to their operation states such as the steady-state output power and operation modes [12]-[15]. Quantitative expression of the FR capabilities of multi-source converters is necessary to incorporate the FR capabilities of multi-source converters into frequency-constrained scheduling. The on/off state of SGs and the operation states of multi-source converters are coupled and should be determined beforehand if the frequency dynamic is considered in the scheduling models.

In this study, we explore an enhanced frequency-constrained scheduling framework considering the support of multi-source converters. The variable FR capabilities of WTG and BES in different modes are modeled, and their operation and control parameters are determined by solving an integrated frequency-constrained scheduling model. The timescale of the model built in this work is day-ahead scheduling including UC, and it is also applicable to intraday ED. Furthermore, the constraints of frequency nadir are often linearized in the frequency-constrained scheduling model, but the error caused by linearization has not been explored in existing works. We discuss the approximation accuracy of the linearized frequency nadir constraints and propose a strategy to reduce the approximation error.

Frequency security constraints have recently been considered in scheduling models. One of the first frequency-constrained UC models was proposed in [16] to ensure sufficient primary FR capabilities, but the frequency dynamics were not established and the frequency nadir constraint was omitted. References [17] and [18] built a UC model and adjusted its results by testing whether the frequency nadir constraint was met. However, the transient simulation needed to be implemented repeatedly in the model, which was complex and time-consuming. A frequency-constrained UC model considering the dynamic ramp rate was built in [19] and solved by binary particle swarm optimization, but the heuristic algorithm could not guarantee the optimality of the solution. Further, [20] modeled frequency dynamics using deep learning, but numerous timing simulations and historical operation data were needed. Reference [21] added linearized frequency nadir constraints to traditional UC models, but the approximation accuracy of linearized equations was not discussed. Reference [22] integrated frequency control into a UC problem for an isolated microgrid, and [23] considered FR from smart loads. The primary and secondary frequency responses of high-voltage direct current (HVDC) were modeled and encoded into a UC model in [24]. However, the FR capabilities of RE were neglected in these works, and frequency security was difficult to establish due to diminishing SG.

To compensate for the FR shortage, the FR capabilities provided by converter-based power electronic interfaces have been explored in frequency-constrained scheduling models. FR provided by RE was integrated into a frequency-constrained UC and ED model in [25]-[29]; in these works, WTG was treated as a virtual synchronous machine with fixed FR parameters, without consideration of its variable FR capabilities depending on wind conditions. References [30] and [31] paid attention to the time-varying FR capabilities of WTG, but WTG only provided a single inertial [30] or droop [31] response. The dynamic interactions of WTG were built into a two-stage frequency-constrained UC in [32]. The contribution of WTG to frequency support was analyzed in a robust scheduling model [33]. Three kinds of WTG de-loading strategies were embedded into a planning model in [34]; however, WTG operates in a de-loading state at a high cost of wind curtailment, which may be unacceptable for utilization. References [35]-[39] proposed frameworks for the scheduling and planning of BES with consideration of fast frequency support. Nonetheless, the coordination of operation states and FR strategies for multi-source converters was not fully exploited by these works.

FR capabilities can be provided by multi-source converters [40], especially from variable-speed WTG and BES. The two main strategies for WTG to provide frequency support are the power unreserved mode (PURM) and the power reserved mode (PRM) [41]-[43]. WTG under the PURM works in the MPPT mode [44], which can provide temporary power increments by releasing the kinetic energy in the rotor [45]. The PRM requires WTG to operate in load-shedding schemes [46], which can supply sufficient and continuous FR at the cost of wind curtailment. BES can provide a rapid and lasting response to the grid frequency deviation [47]-[50] through the controller to compensate for the imbalanced power.

The coordinated control of frequency support capabilities from WTG and BES was proposed in [51]-[54] to reduce wind power curtailment and improve the FR effect. However, these efforts were not effectively integrated with the frequency-constrained scheduling model. FR performance and economic operation are related to the working states, operation modes, and parameters of FR provided by WTG and BES. These factors are complexly coupled together, and a new method needs to be established to coordinate both strategies and the working states of BES and WTG to provide FR.

In summary, the existing frequency-constrained scheduling models largely simplify or ignore the coupling of variable FR capabilities and working states from multi-source converters. In addition, the accuracy of linearized frequency security constraints has not been analyzed. In this study, we propose a frequency-constrained scheduling model considering FR capabilities from WTG and BES. An iteration-based strategy is designed to improve the approximation accuracy of the frequency nadir constraints.

The contributions of this study can be summarized as follows.

1) Quantitative expression of the FR capabilities of multi-source converters is given. The FR capabilities and variable control parameters of WTG under both the PURM and the PRM are modeled. WTG is allowed to adjust the frequency support modes and control parameters to reduce wind curtail-

ment as much as possible as long as it meets specified conditions satisfying the requirements for FR. Multi-target allocation of BES capacity between tracking dispatch instruction and emergency FR is considered. The reserved power and capacity required for BES to provide emergency FR are calculated and embedded into the model.

2) An enhanced frequency-constrained scheduling model incorporating variable frequency support capabilities of multi-source converters is established. Frequency dynamic indices are analytically expressed considering the support from both SGs and multi-source converters. Variable FR capabilities of WTG and BES are embedded into the integrated frequency-constrained scheduling model. FR modes and parameters of multi-source converters are determined in the scheduling model.

3) A strategy for improving the approximation accuracy of the linearized frequency nadir constraints is proposed.

The remainder of this paper is organized as follows. Section II models the quantitative expressions of the FR capabilities of WTG and BES. Section III establishes the aggregated frequency dynamic functions, linearizes the frequency security constraints, and details the proposed method to improve the linearization accuracy. Section IV builds the integrated frequency-constrained scheduling model. Section V presents the case studies, and Section VI offers the conclusions of this study.

## II. Frequency Dynamic Responses with Variable FR Parameters of Multi-source Converters

Unlike SGs that can support stable inertia and frequency droop responses naturally under an "on" state, FR capabilities provided by converter-based WTG and BES are related to their operation points and customized FR control strategies. In this section, the operation modes and parameters of FR provided by multi-source converters are incorporated into frequency dynamic models, which can be easily integrated into the traditional SG-dominated second-order frequency dynamic function. WTG and BES in this paper are modeled as grid-following converters with frequency support controllers. The output power of multi-source converters could change with the frequency measured by their phase-locked loops (PLLs), providing frequency support for the system.

### A. Frequency Support from WTG

#### 1) Frequency Response Under PRM

WTG working under the PRM is believed to provide lasting frequency support. The reserved wind power is shared with both virtual inertia and droop control strategies. The power increment of WTG under the PRM $\Delta P_w^{PRM}$ is expressed as:

$$\Delta P_w^{PRM} = -2H^{PRM}\frac{\mathrm{d}\Delta f}{\mathrm{d}t} - K^{PRM}\Delta f \tag{1}$$

The power increment $\Delta P_w^{PRM}$ should not exceed the reserved wind power $R_w^W$. We assume that $R_w^W$ is divided into two parts, i.e., $R_w^{W,H}$ for inertia support and $R_w^{W,K}$ for droop support. Inspired by [34], $H^{PRM}$ and $K^{PRM}$ are given in (2) to ensure that $\Delta P_w^{PRM}$ does not exceed $R_w^W$.

$$\begin{cases} H^{PRM} = \dfrac{R_w^{W,H}}{2\left|ROCOF_{\max,set}\right|} \\ K^{PRM} = \dfrac{R_w^{W,K}}{\left|\Delta f_{nadir,set}\right|} \end{cases} \tag{2}$$

The values of $R_w^{W,H}$ and $R_w^{W,K}$ are set as variables to be optimized in the later scheduling model, so $H^{PRM}$ and $K^{PRM}$ in this study are time-varying FR parameters to be determined according to the later scheduling model.

#### 2) Frequency Response Under PURM

Under the PURM, WTG works in the MPPT mode without sacrificing wind power capture. WTG under the PURM participates in FR through virtual inertial control [55], [56], whose virtual inertial constant $H^{PURM}$ is given as:

$$H^{PURM} = \begin{cases} \dfrac{\omega^2 - \omega_{\min}^2}{\omega_{\max}^2 - \omega_{\min}^2} H_{rated}^{PURM} & \omega > \omega_{\min} \\ 0 & \omega \le \omega_{\min} \end{cases} \tag{3}$$

The power increment of WTG under the PURM $\Delta P_w^{PURM}$ is expressed as:

$$\Delta P_w^{PURM} = -2H^{PURM}\frac{\mathrm{d}\Delta f}{\mathrm{d}t} \tag{4}$$

Figure 1 shows the frequency controllers of WTG under the PRM and PURM. WTG is assumed to be equipped with these two controllers, and one controller is chosen during each scheduling period for frequency support. The proportion of WTG under the PRM or PURM during each scheduling period is set as the optimization variable in the later scheduling model.

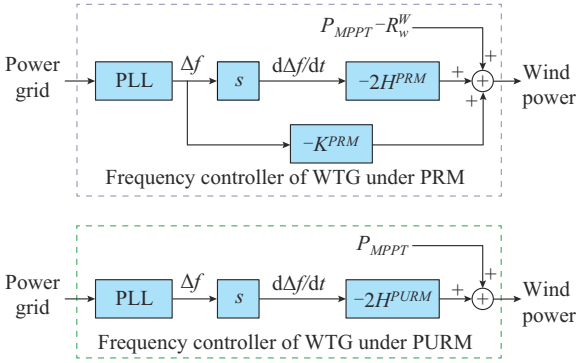


Fig. 1. Frequency controllers of WTG under PRM and PURM.

### B. Frequency Support from BES

BES is equipped with a frequency controller that can actively change the output power according to the system frequency measured by a PLL. The power-frequency controller of BES is shown in Fig. 2.

BES tracks dispatch instructions from the dispatch center and provides frequency support through its frequency controller. When the system suffers a serious frequency contingency, the ROCOF or frequency deviation exceeds a certain threshold, and the frequency controller will convert to emergency frequency support mode until the frequency dynamics process in the system ends. When detecting a serious low-frequency contingency in the system, BES will discharge at

the maximum power $P_b^{B,\max}$ immediately [35], [36] after switching to emergency frequency support mode. Assume that a contingency occurs at $t=0$ s, and the dispatch instruction for BES at the moment before the contingency is $P_b^B\big|_{t=0^-}$ (positive means charging and negative means discharging), which satisfies $-P_b^{B,\max} \le P_b^B\big|_{t=0^-} \le P_b^{B,\max}$. The power increment that BES can provide is $P_b^{B,\max} + P_b^B\big|_{t=0^-}$, which ranges from 0 to $2P_b^{B,\max}$. To prevent the power increment provided by BES from being greater than the system power shortage, which may cause overcompensation, the ROCOF threshold to trigger the emergency frequency support mode can be set as:

$$ROCOF_{threshold} = \frac{P_b^{B,\max}}{\underline{H}^{SYS}} \tag{5}$$

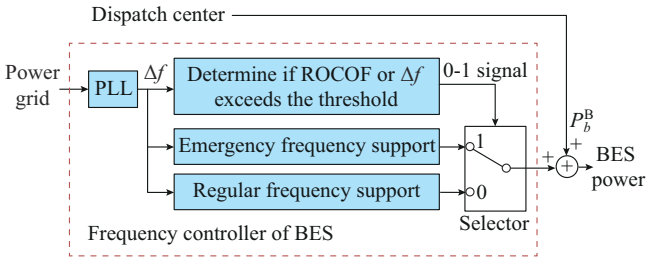


Fig. 2. Power-frequency controller of BES.

The setting of $ROCOF_{threshold}$ can ensure that BES will not overcompensate during emergency frequency support, which is proven in (6).

$$P_{IM} = 2ROCOF \cdot H^{SYS} \ge 2ROCOF_{threshold} \cdot H^{SYS} = \frac{2P_b^{B,\max} H^{SYS}}{\underline{H}^{SYS}} \ge 2P_b^{B,\max} \ge P_b^{B,\max} + P_b^B\big|_{t=0^-} \tag{6}$$

Since it takes minutes to recover the system frequency after a contingency, BES needs to continuously provide frequency support. Under the emergency frequency support mode, BES is set to discharge at its maximum power $P_b^{B,\max}$ during $0 \le t < T_b^{ir}$ and provides continuous power support $P_b^{B,end}$ until $T_b^{end}$. To prevent a secondary frequency drop caused by the sudden power change of BES, we set the output power of BES to change linearly during $[T_b^{ir}, T_b^{pfr}]$ from $-P_b^{B,\max}$ to $-P_b^{B,end}$. In this study, $T_b^{ir}$, $T_b^{pfr}$, and $T_b^{end}$ are set as 15 s, 60 s, and 15 min, respectively. Neglecting the response time of the frequency measurement devices and BES controller, the BES power increment $\Delta P_b^B(t)$ under the emergency frequency support mode can be expressed as (7), and the output power of BES $P_b^B(t)$ under emergency frequency support mode is shown in Fig. 3.

$$\Delta P_b^B(t) = \begin{cases} P_b^{B,\max} + P_b^B\big|_{t=0^-} & 0 \le t < T_b^{ir} \\ P_b^{B,\max} + \dfrac{(t-T_b^{ir})(P_b^{B,end} - P_b^{B,\max})}{T_b^{pfr} - T_b^{ir}} + P_b^B\big|_{t=0^-} & T_b^{ir} \le t \le T_b^{pfr} \\ P_b^{B,end} + P_b^B\big|_{t=0^-} & T_b^{pfr} < t \le T_b^{end} \end{cases} \tag{7}$$

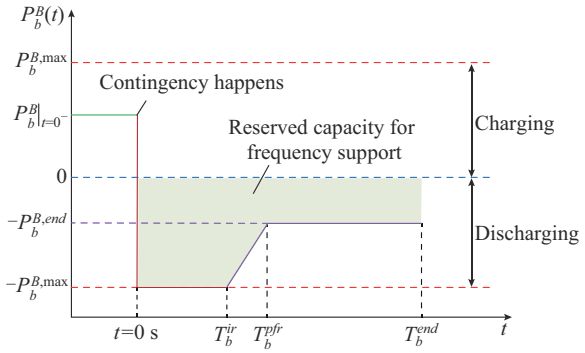


Fig. 3. Output power of BES under emergency frequency support mode.

Assuming that a contingency occurs during the $p^{\text{th}}$ scheduling period, during which BES operates with dispatch instruction power $P_{b,p}^B$, we have:

$$P_b^B\big|_{t=0^-} = P_{b,p}^B \tag{8}$$

To ensure that BES has enough energy for the emergency frequency support mode, as shown in Fig. 3, the reserved capacity $E_b^{B,f}$ for frequency support BES is calculated as:

$$E_b^{B,f} = \frac{\int_0^{T_b^{end}} P_b^B(t)\mathrm{d}t}{\eta_b^{dis}} = \frac{(T_b^{ir} + T_b^{pfr})(P_b^{B,\max} - P_b^{B,end})/2 + T_b^{end} P_b^{B,end}}{\eta_b^{dis}} \tag{9}$$

The dispatch instruction power $P_{b,p}^B$, continuous power support $P_b^{B,end}$, and reserved capacity $E_b^{B,f}$ of BES are set as variables to be optimized in the later scheduling model.

## III. Frequency Dynamic and Security Constraints Considering Multi-source Converters

In this section, the aggregated frequency dynamic functions considering multi-source converters are given, and the frequency security constraints are formulated. The frequency dynamics are analyzed based on three pivotal frequency dynamic indices of ROCOF, frequency nadir $f_{nadir}$, and steady-state frequency $f_{ss}$ after contingency. Considering that a linear simplified model is used in the calculation, the linearization accuracy is also discussed, and an iteration-based strategy is proposed for improving the accuracy level.

### *A. Aggregated Frequency Dynamic Functions*

Assuming the system suffers a contingency occurring during the $p^{\text{th}}$ scheduling period at $t=0$, and the contingency causes instantaneous imbalanced power with the amount of $P_{IM}$ at $t=0$, WTG under the PRM and PURM provides power increments of $\Delta P_w^{PRM}$ and $\Delta P_w^{PURM}$, respectively, and BES gives a frequency support power of $\Delta P_b^B$. The frequency dynamic function of the system is expressed as:

$$\begin{cases} 2H^G \dfrac{\mathrm{d}\Delta f(t)}{\mathrm{d}t} = -(P_{IM} - \Delta P_w^{PRM} - \Delta P_w^{PURM} - \Delta P^G - \Delta P^L - \Delta P_b^B) \\ T^G \dfrac{\mathrm{d}\Delta P^G(t)}{\mathrm{d}t} + \Delta P^G(t) = -K^G \Delta f(t) \\ \Delta P^L(t) = -K^L \Delta f(t) \end{cases} \tag{10}$$

The aggregated system frequency model is shown in Fig. 4, and the frequency dynamic process can be expressed as (11), which is a second-order differential equation.

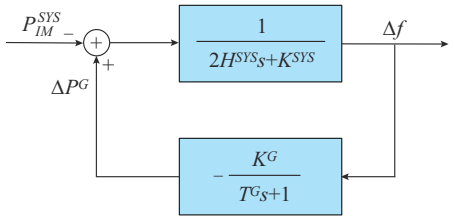


Fig. 4. Aggregated system frequency model.

$$2T^G H^{SYS}\frac{\mathrm{d}^2\Delta f(t)}{\mathrm{d}t^2}+(2H^{SYS}+T^G K^{SYS})\frac{\mathrm{d}\Delta f(t)}{\mathrm{d}t}+K^{SS}\Delta f(t)+P_{IM}^{SYS}=0 \tag{11}$$

$$\begin{cases} H^{SYS}=H^G+H^{PRM}+H^{PURM} \\ K^{SYS}=K^L+K^{PRM} \\ K^{SS}=K^{SYS}+K^G \\ P_{IM}^{SYS}=P_{IM}-\Delta P_b^B \\ \Delta P_b^B=P_b^{B,\max}+P_{b,p}^B \end{cases} \tag{12}$$

The initial conditions are given as:

$$\begin{cases} \Delta f(0)=0 \\ \left.\dfrac{\mathrm{d}\Delta f(t)}{\mathrm{d}t}\right|_{t=0^+}=-\dfrac{P_{IM}^{SYS}}{2H^{SYS}} \end{cases} \tag{13}$$

The discriminant $\Lambda$ for determining whether the two-order dynamic system is underdamped or overdamped is given as:

$$\Lambda=(2H^{SYS}+T^G K^{SYS})^2-8T^G H^{SYS}K^{SS} \tag{14}$$

According to the value of $\Lambda$, the system may have three kinds of FR modes: overdamped ($\Lambda>0$), critical damped ($\Lambda=0$), and underdamped ($\Lambda<0$) responses.

*1) Overdamped Response*

The frequency of the overdamped response can be solved as:

$$\Delta f(t)=-P_{IM}^{SYS}(C_1\mathrm{e}^{-(\alpha-\Omega)t}+C_2\mathrm{e}^{-(\alpha+\Omega)t}+1/K^{SS}) \tag{15}$$

$$\begin{cases} \alpha=[1/T^G+K^{SYS}/(2H^{SYS})]/2 \\ \Omega=\sqrt{\left|K^{SS}/(2H^{SYS}T^G)-\alpha^2\right|} \\ C_1=1/(4\Omega H^{SYS})-\alpha/(2\Omega K^{SS})-1/(2K^{SS}) \\ C_2=-1/(4\Omega H^{SYS})+\alpha/(2\Omega K^{SS})-1/(2K^{SS}) \end{cases} \tag{16}$$

A frequency nadir is reached at $t_{nadir}$, as expressed in (17), which can be obtained by solving $\mathrm{d}f(t)/\mathrm{d}t=0$.

$$t_{nadir}=\frac{1}{2\Omega}\ln\frac{C_2(\Omega+\alpha)}{C_1(\Omega-\alpha)} \tag{17}$$

*2) Critical Damped Response*

The frequency of the critical damped response can be solved by:

$$\Delta f(t)=-P_{IM}^{SYS}(D_1\mathrm{e}^{-\alpha t}+D_2 t\mathrm{e}^{-\alpha t}+1/K^{SS}) \tag{18}$$

$$\begin{cases} D_1=-\dfrac{1}{K^{SS}} \\ D_2=\dfrac{1}{2H^{SYS}}-\dfrac{\alpha}{K^{SS}} \\ t_{nadir}=\dfrac{1}{\alpha}-\dfrac{D_1}{D_2} \end{cases} \tag{19}$$

*3) Underdamped Response*

The frequency of the underdamped response can be solved by:

$$\Delta f(t)=-P_{IM}^{SYS}(1-2A\mathrm{e}^{-\alpha t}\cos(\Omega t+\varphi))/K^{SS} \tag{20}$$

$$\begin{cases} A=\sqrt{K^{SS}K^G}/(4\Omega H^{SYS}) \\ \varphi=\arctan\{[K^{SS}/(2H^{SYS})-\alpha]/\Omega\} \end{cases} \tag{21}$$

Additionally, $t_{nadir}$ can be expressed as:

$$t_{nadir}=(\arctan(-\alpha/\Omega)-\varphi+\pi)/\Omega \tag{22}$$

The lowest frequency $f_{nadir}$ of the system after contingency can be expressed as:

$$f_{nadir}=f_0+\Delta f(t_{nadir}) \tag{23}$$

## B. Frequency Security Constraints

The frequency security constraints of ROCOF, steady-state frequency, and frequency nadir are modeled. The linearization method of the frequency nadir constraint and the strategy for improving its approximation accuracy are given.

*1) ROCOF Constraints*

ROCOF is limited to not exceeding $\left|ROCOF_{\max,set}\right|$, and the ROCOF constraint is a linear inequality about $P_{IM}^{SYS}$ and $H^{SYS}$.

$$P_{IM}^{SYS}\le 2\left|ROCOF_{\max,set}\right|H^{SYS} \tag{24}$$

*2) Steady-state Frequency Constraints*

When $t>T_b^{pfr}$, the frequency tends to be stable, and the output power of BES is $P_b^{B,end}$ instead of discharging at rated power $P_b^{B,\max}$. $P_{IM}^{SYS,end}$ is set in (25) as the imbalanced power when the frequency of the system becomes stable.

$$P_{IM}^{SYS,end}=P_{IM}-P_b^{B,end}-P_{b,p}^B \tag{25}$$

The value of $f_{ss}$ is defined as:

$$f_{ss}=f_0-\frac{P_{IM}^{SYS,end}}{K^{SS}} \tag{26}$$

The constraint of $f_{ss}$ is shown in (27), which is equal to a linear constraint expressed as (28).

$$f_{ss}\ge\left|f_{ss,set}\right| \tag{27}$$

$$P_{IM}^{SYS,end}\le\left(f_0-\left|f_{ss,set}\right|\right)K^{SS} \tag{28}$$

*3) Frequency Nadir Constraints*

The maximum frequency deviation $\left|\Delta f(t_{nadir})\right|$ after contingency must not be higher than the set value $\left|\Delta f_{nadir,set}\right|$ to avoid triggering low-frequency load shedding, and the frequency nadir constraint can be expressed as:

$$\left|\Delta f(t_{nadir})\right|\le\left|\Delta f_{nadir,set}\right| \tag{29}$$

The expression of $\chi$, which is a function of variables $H^{SYS}$, $K^{SYS}$, and $K^G$, is defined in (30), and the constraint (29) is

equivalent to (31).

$$\chi(H^{SYS},K^{SYS},K^{G})=\frac{\left|\Delta f_{nadir,set}\right|}{\left|\Delta f(t_{nadir})\right|}P_{IM}^{SYS} \tag{30}$$

$$P_{IM}^{SYS}\le\chi(H^{SYS},K^{SYS},K^{G}) \tag{31}$$

$\chi(H^{SYS},K^{SYS},K^{G})$ is nonlinear to variables $H^{SYS}$, $K^{SYS}$, and $K^{G}$, which makes it difficult to embed the frequency nadir constraints into the scheduling model. Inspired by [26] and [27], we assume that the domain of definition of $\chi(H^{SYS},K^{SYS},K^{G})$ is $\Gamma=\{(H^{SYS},K^{SYS},K^{G})\}$, and we divide $\Gamma$ into a series of subspaces $\Gamma_m$ $(m=1,2,...,M)$. In each subspace, the linear equations $L_m^{\chi}$ $(m=1,2,...,M)$ are built as the lower bound to approximate $\chi(H^{SYS},K^{SYS},K^{G})$. The combining parameters of the $m^{\text{th}}$ linear equation are $\pi_m^{Hsys}$, $\pi_m^{Ksys}$, $\pi_m^{Kg}$, and $\pi_m^{B}$. $\pi=\{(\pi_m^{Hsys},\pi_m^{Ksys},\pi_m^{Kg},\pi_m^{B})\}_{m=1}^{M}$ can be obtained by constrained quadratic programming expressed as:

$$\min_{\pi}\left\{\sum_{m=1}^{M}\sum_{(H^{SYS},K^{SYS},K^{G})\in\Gamma_m}(L_m^{\chi}-\chi(H^{SYS},K^{SYS},K^{G}))^2\right\} \tag{32}$$

s.t.

$$L_m^{\chi}\le\chi(H^{SYS},K^{SYS},K^{G})\quad\forall m \tag{33}$$

$$L_m^{\chi}=\pi_m^{Hsys}H^{SYS}+\pi_m^{Ksys}K^{SYS}+\pi_m^{Kg}K^{G}+\pi_m^{B} \tag{34}$$

After obtaining the optimal parameter $\hat{\pi}$, $\underline{\chi}$ in (35) is a linear lower bound of $\chi$.

$$\underline{\chi}(H^{SYS},K^{SYS},K^{G})=\min_{m=1,2,...,M}L_m^{\chi}(H^{SYS},K^{SYS},K^{G}|\hat{\pi}) \tag{35}$$

Then, the frequency nadir constraint can be converted into a series of linear constraints shown in (36), which is stronger than the original constraint (31).

$$P_{IM}^{SYS}\le\underline{\chi}(H^{SYS},K^{SYS},K^{G}) \tag{36}$$

1) Approximation accuracy of linearization

We set the definition domain of the variables in $\chi$ as $H^{SYS}\in[2,10]$ s, $K^{SYS}\in[1,6]$, and $K^{G}\in[5,20]$, which covers broad scenarios, where the SG capacity accounts for 25% to 100% of the system. The number of interval subspaces for linearization is set to be $M=160$. The comparison of the original function $\chi(H^{SYS},K^{SYS},K^{G})$ and the calculated linearized lower bound $\underline{\chi}(H^{SYS},K^{SYS},K^{G})$ is shown in Fig. 5.

Figure 5 shows that the approximation error caused by linearization increases with the decrease of $H^{SYS}$ and $K^{G}$ (caused by the decrease of SG capacity), reaching the maximum error rate of 7.9% when $H^{SYS}=2$ s and $K^{G}=5$. This reflects that when the proportion of SGs is lower, the nonlinearity of the original function $\chi(H^{SYS},K^{SYS},K^{G})$ is enhanced, and the error caused by the linearization method will be larger.

2) Accuracy improvement strategy

The frequency nadir constraints will be accurate if the optimal solutions of the variables obtained by the scheduling model are within the range of the set of subspaces $\Gamma_m$. On the premise of ensuring that the solutions are within the set of subspaces, reducing the size of the definition domain can effectively remove unnecessary constraints. The shape of $\chi$ near the optimal solution is better focused, and the strength of the constraints decreases.

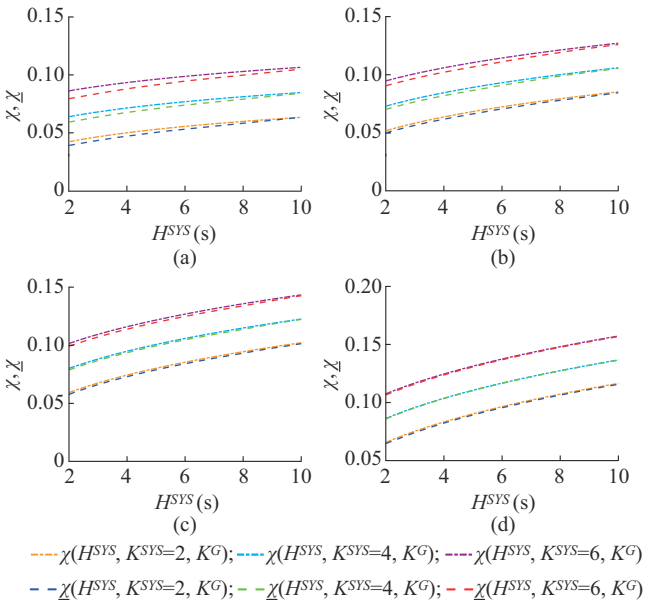


Fig. 5. Comparison between original function and its linearized lower bound. (a) $K^{G}=5$. (b) $K^{G}=10$. (c) $K^{G}=15$. (d) $K^{G}=20$.

An iteration-based strategy for improving the accuracy of the linearized frequency nadir constraints is proposed, and the flowchart of the strategy is shown in Fig. 6. With the proposed strategy, the size of the definition domain diminishes by $\varepsilon$ through each iteration and the error caused by linearization decreases.

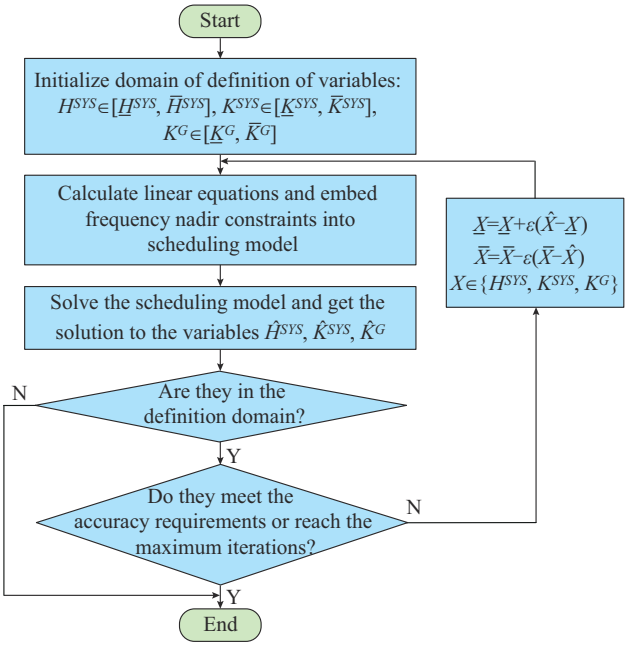


Fig. 6. Flowchart of proposed iteration-based strategy for improving approximation accuracy of linearized frequency nadir constraints.

## IV. Day-ahead Scheduling Model with Frequency Security Constraints Coordinating Frequency Support from Multi-source Converters

A frequency-constrained day-ahead scheduling model considering the FR capabilities of WTG and BES is established

in this section. First, we present a typical day-ahead scheduling model including UC. Then, we embed frequency security constraints and FR capabilities of multi-source converters into the scheduling model.

### A. Typical Day-ahead Scheduling

#### 1) Objective Function

The objective of the day-ahead scheduling model is to minimize the operation cost, including the SG operation cost, BES operation cost, and load shedding cost.

$$\min C_{sys}=\sum_{i=1}^{N_I}Pr_i\cdot\sum_{p=1}^{N_P}\Bigg[\sum_{g=1}^{N_G}(C_g^{su}u_{g,p}^{su}+C_g^{sd}u_{g,p}^{sd}+C_g^{nl}u_{g,p}+C_g^{gen}P_{g,p,i}^{G})+\sum_{n=1}^{N_N}C_lP_{n,p,i}^{L,loss}+\sum_{b=1}^{N_B}(C_b^{dis}P_{b,p,i}^{B,dis}+C_b^{ch}P_{b,p,i}^{B,ch})\Bigg] \tag{37}$$

#### 2) Constraints

Equation (38) represents the bus active power balance constraints. Equation (39) limits the RE curtailment and load shedding. Equation (40) is the DC power flow model representing the thermal limits of the circuits.

$$\sum_{g\in\Omega_n^G}P_{g,p,i}^{G}+\sum_{w\in\Omega_n^W}(P_{w,p,i}^{W}-P_{w,p,i}^{W,loss})+\sum_{pv\in\Omega_n^{PV}}(P_{pv,p,i}^{PV}-P_{pv,p,i}^{PV,loss})-\sum_{l\in\Omega_n^{LS}}L_{l,p,i}+\sum_{l\in\Omega_n^{LE}}L_{l,p,i}=P_{n,p}^{L}-P_{n,p,i}^{L,loss}+\sum_{b\in\Omega_n^{B}}P_{b,p,i}^{B}\quad\forall n,p,i \tag{38}$$

$$\begin{cases}0\le P_{w,p,i}^{W,loss}\le P_{w,p,i}^{W}\quad\forall w,p,i\\0\le P_{pv,p,i}^{PV,loss}\le P_{pv,p,i}^{PV}\quad\forall pv,p,i\\0\le P_{n,p,i}^{L,loss}\le P_{n,p}^{L}\quad\forall n,p,i\end{cases} \tag{39}$$

$$\begin{cases}L_{l,p,i}=(\theta_{l(+),p,i}-\theta_{l(-),p,i})/x_l\quad\forall l,p,i\\\left|\theta_{n,p,i}\right|\le\theta_{\max}\quad\forall n,p,i\\\left|L_{l,p,i}\right|\le L_{l,\max}\quad\forall l,p,i\end{cases} \tag{40}$$

Equation (41) gives the operation constraints of the SGs.

$$\begin{cases}u_{g,p}P_g^{G,\min}\le P_{g,p,i}^{G}\le u_{g,p}P_g^{G,\max}\quad\forall g,p,i\\u_{g,p-1}=u_{g,p}+u_{g,p}^{sd}-u_{g,p}^{su}\quad\forall g,p\\P_{g,p,i}^{G}-P_{g,p-1,i}^{G}\le u_{g,p-1}R_g^{up}+u_{g,p}^{su}P_g^{G,\min}\quad\forall g,p,i\\P_{g,p-1,i}^{G}-P_{g,p,i}^{G}\le u_{g,p}R_g^{dn}+u_{g,p}^{sd}P_g^{G,\min}\quad\forall g,p,i\\\sum_{\tau=p-T_g^{on}-1}^{p-1}u_{g,\tau}\ge u_{g,p}^{sd}T_g^{on}\quad\forall g,p\\\sum_{\tau=p-T_g^{off}-1}^{p-1}(1-u_{g,\tau})\ge u_{g,p}^{su}T_g^{off}\quad\forall g,p\end{cases} \tag{41}$$

Equation (42) is the system reserve constraint.

$$\sum_g u_{g,p}P_g^{G,\max}+\sum_w P_{w,p,i}^{W}+\sum_{pv}P_{pv,p,i}^{PV}+\sum_b P_b^{B,\max}\ge(1+r_L)\sum_n P_{n,p}^{L}+r_{RE}\left(\sum_w P_{w,p,i}^{W}+\sum_{pv}P_{pv,p,i}^{PV}\right)\quad\forall p,i \tag{42}$$

Equations (43) and (44) are the operation constraints of BES.

$$\begin{cases}P_{b,p,i}^{B}=P_{b,p,i}^{B,ch}-P_{b,p,i}^{B,dis}\quad\forall b,p,i\\0\le P_{b,p,i}^{B,ch}\le u_{b,p,i}^{ch}P_b^{B,\max}\quad\forall b,p,i\\0\le P_{b,p,i}^{B,dis}\le u_{b,p,i}^{dis}P_b^{B,\max}\quad\forall b,p,i\\\left|P_{b,p,i}^{B}-P_{b,p-1,i}^{B}\right|\le R_b^{B}\quad\forall b,p,i\\u_{b,p,i}^{ch}+u_{b,p,i}^{dis}\le 1\quad u_{b,p,i}^{ch},u_{b,p,i}^{dis}\in\{0,1\},\ \forall b,p,i\end{cases} \tag{43}$$

$$\begin{cases}E_{b,p+1,i}^{B}=E_{b,p,i}^{B}+P_{b,p,i}^{B,ch}\eta_b^{ch}-P_{b,p,i}^{B,dis}/\eta_b^{dis}\quad\forall b,p,i\\E_{b,1,i}^{B}=E_{b,N_p,i}^{B}\quad\forall b,i\\SOC_b^{\min}\cdot E_b^{B,\max}\le E_{b,p,i}^{B}\le SOC_b^{\max}\cdot E_b^{B,\max}\quad\forall b,p,i\end{cases} \tag{44}$$

### B. Constraints Representing Frequency Support from BES and WTG

#### 1) Constraints Representing Frequency Support from WTG

As introduced in Section II, WTG provides frequency support under the PRM or PURM; the proportion of WTG under the PRM during the $p^{\text{th}}$ scheduling period is set to be $\beta_{w,p,i}$, and the remaining WTG provides frequency support under the PURM. WTG under the PRM provides frequency support using part of the wind curtailment. Equation (45) ensures that the wind curtailment is no more than the theoretical wind power under the PRM. Equation (46) limits the reserved power $R_{w,p,i}^{W}$. Equation (47) means that the reserved power is shared with $R_{w,p,i}^{W,H}$ for inertia support and $R_{w,p,i}^{W,K}$ for droop support.

$$\begin{cases}0\le P_{w,p,i}^{W,loss}\le\beta_{w,p,i}P_{w,p,i}^{W}\\0\le\beta_{w,p,i}\le 1\end{cases} \tag{45}$$

$$0\le R_{w,p,i}^{W}\le P_{w,p,i}^{W,loss} \tag{46}$$

$$\begin{cases}R_{w,p,i}^{W}=R_{w,p,i}^{W,H}+R_{w,p,i}^{W,K}\\R_{w,p,i}^{W,H}\ge 0\\R_{w,p,i}^{W,K}\ge 0\end{cases} \tag{47}$$

According to (2), the virtual inertia $H_{p,i}^{PRM}$ and droop constant $K_{p,i}^{PRM}$ provided by the aggregated WTG controller under the PRM are expressed as (48). Considering the fluctuation of wind power within hours, the FR parameters of wind power are corrected by the lower bound of its output power within hours to ensure sufficient FR capabilities. The method of obtaining the lower bound and calculating the coefficient of correction can be seen in [34].

$$\begin{cases}H_{p,i}^{PRM}=\sum_w\dfrac{R_{w,p,i}^{W,H}f_0}{2\left|ROCOF_{\max,set}\right|S_{sys}}\xi_{p,i}\\K_{p,i}^{PRM}=\sum_w\dfrac{R_{w,p,i}^{W,K}f_0}{\left|\Delta f_{nadir,set}\right|S_{sys}}\xi_{p,i}\end{cases} \tag{48}$$

The virtual inertia $H_{p,i}^{PURM}$ provided by the aggregated WTG controller under the PRM is expressed as:

$$H_{p,i}^{PURM}=\sum_w\frac{(1-\beta_{w,p,i})S_wH_w^{PURM}}{S_{sys}}\xi_{p,i} \tag{49}$$

#### 2) Constraints Representing Frequency Support from BES

Frequency support from BES is considered in the frequency security constraints. As shown in (9), the reserved BES capacity $E_{b,p,i}^{B,f}$ for providing FR is expressed as (50), and the

remaining BES capacity constraints are further expressed as (51).

$$E_{b,p,i}^{B,f}=\frac{(T_{b,p,i}^{ir}+T_{b,p,i}^{pfr})(P_b^{B,\max}-P_{b,p,i}^{B,end})/2+T_{b,p,i}^{end}P_{b,p,i}^{B,end}}{\eta_b^{dis}} \tag{50}$$

$$SOC_b^{\min}\cdot E_b^{B,\max}+E_{b,p,i}^{B,f}\le E_{b,p,i}^{B}\le SOC_b^{\max}\cdot E_b^{B,\max} \tag{51}$$

Assume the system may suffer a contingency causing instantaneous imbalanced power with the amount of $P_{IM,p,i}$. Through the emergency frequency response control of BES, which is expressed in (7), the initial imbalanced power $P_{IM,p,i}^{SYS}$ and the steady-state imbalanced power $P_{IM,p,i}^{SYS,end}$ can be expressed as:

$$\begin{cases}P_{IM,p,i}^{SYS}=P_{IM,p,i}-\sum_b(P_b^{B,\max}+P_{b,p,i}^{B})\\ P_{IM,p,i}^{SYS,end}=P_{IM,p,i}-\sum_b(P_b^{B,end}+P_{b,p,i}^{B})\end{cases} \tag{52}$$

### C. Frequency Security Constraints Under Day-ahead Scheduling

The contingency is considered as the largest $N-1$ fault of the online generators, DC line injection trip-off, or instantaneous load increment, and it brings instantaneous imbalanced power $P_{IM,p,i}$. Note that if the faulty generator has FR capability, its FR parameters need to be set as zero in the subsequent frequency dynamic equation.

The inertia constant $H_p^G$ and droop constant $K_p^G$ provided by the aggregated SG depend on the SG on/off state, which are expressed as:

$$\begin{cases}H_p^G=\sum_{g=1}^{N_G}S_gH_gx_{g,p}^G/S_{sys} & \forall p\\ K_p^G=\sum_{g=1}^{N_G}S_gK_gx_{g,p}^G/S_{sys} & \forall p\end{cases} \tag{53}$$

The aggregate frequency response parameters in (11) for each RE scenario $i$ and scheduling period $p$ are shown as:

$$\begin{cases}H_{p,i}^{SYS}=H_p^G+H_{p,i}^{PRM}+H_{p,i}^{PURM}\\ K_{p,i}^{SYS}=K_{p,i}^{L}+K_{p,i}^{PRM}\\ K_{p,i}^{G}=K_p^G\\ K_{p,i}^{SS}=K_{p,i}^{SYS}+K_{p,i}^{G}\end{cases} \tag{54}$$

According to (24), (28), and (36), the linear frequency security constraints for ROCOF, frequency nadir, and steady-state frequency for each RE scenario $i$ and scheduling period $p$ are further expressed as:

$$\begin{cases}P_{IM,p,i}^{SYS}\le 2\left|ROCOF_{\max,set}\right|H_{p,i}^{SYS} & \forall p,i\\ P_{IM,p,i}^{SYS,end}\le(f_0-\left|f_{ss,set}\right|)K_{p,i}^{SS} & \forall p,i\\ P_{IM,p,i}^{SYS}\le\underline{\chi}(H_{p,i}^{SYS},K_{p,i}^{SYS},K_{p,i}^{G}) & \forall p,i\end{cases} \tag{55}$$

The frequency response modes and parameters of WTG and BES are determined by solving the integrated scheduling optimization model. The above optimization model of the frequency-constrained day-ahead optimal scheduling model is a standard mixed-integer linear programming (MILP) problem that can be effectively solved by the existing solvers.

## V. Case Study

### A. Test System

We analyze the proposed scheduling model on a modified IEEE 24-bus standard test system presented in Fig. 7. The time resolution of the day-ahead scheduling is 1 hour. The constant time of the SG speeder is $T^G=5$ s, and the other parameters of the SGs are shown in Table I. The base capacity of the system is set to be 10000 MW, and the frequency droop coefficient of the load is $K^L=2$ p.u.. The frequency security requirements are set to be $\left|ROCOF_{\max,set}\right|=0.4$ Hz/s, $\left|f_{nadir,set}\right|=49.4$ Hz, and $\left|f_{ss,set}\right|=49.7$ Hz. The contingency of the case study is considered as applying an 8% instantaneous load increase, which is equivalent to the generation loss of the same power. Although the imbalanced power caused by the contingency is set as a fixed proportion to the load, it can be expediently extended to the $N-1$ fault of the online generators or DC line injection trip-off through the model built in Section IV.

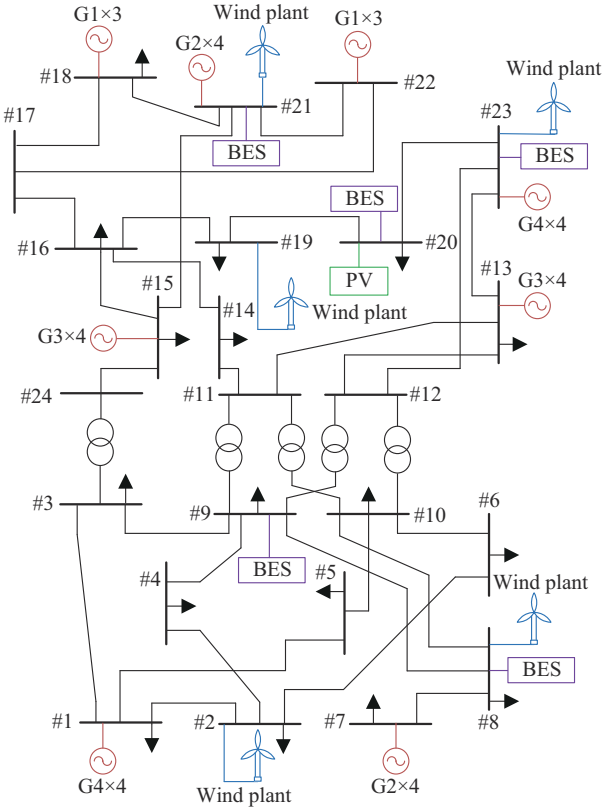


Fig. 7. Structure of modified IEEE 24-bus standard system.

The penetration rates of wind and PV plants are 50% and 10% of the base capacity, respectively. Nine RE scenarios are generated based on day-ahead probabilistic forecasting through the approach proposed in [57] to reflect the uncertainty of renewable generation production. The lower and upper limits of WTG rotor speeds are $\omega_{\min}=0.7$ p.u. and $\omega_{\max}=1.2$ p.u., respectively. The total installed power of BES is 150 MW, which is considered as a 2-hour system. The charging and discharging efficiencies of BES are set to be $\eta_{ch}=\eta_{dis}=0.95$. The lower and upper limits of the state of charge

(SOC) are $SOC_{min}=0.1$ and $SOC_{max}=0.9$, respectively. As shown in Table II, nine cases are set and compared to verify the effectiveness of the proposed model. The scheduling model proposed in this study is Case 3.4, which considers frequency security constraints as well as FR capabilities from BES and WTG under the PURM and PRM. Case 1 is compared with other cases to reflect the impact of frequency security constraints. Cases 2.1-2.4 and Cases 3.1-3.4 are set to compare different strategies of FR from BES and WTG. The simulations are carried out on a computer with an Intel Core i9 processor running at 3.9 GHz with 64 GB of memory. The optimal scheduling model is solved with the GUROBI package in MATLAB R2022b.

TABLE I
PARAMETERS OF SGS

| SG type | Capacity of each unit (MW) | Number of units | Variable cost ($/MWh) | Start-up cost ($/MW) | Shut-down cost ($/MW) | Inertial constant (s) | Frequency droop coefficient (p.u.) |
|---|---|---|---|---|---|---|---|
| G1 | 500 | 6 | 22 | 8 | 8 | 9.6 | 20 |
| G2 | 400 | 8 | 25 | 6 | 6 | 8.3 | 20 |
| G3 | 300 | 8 | 30 | 4 | 4 | 6.7 | 20 |
| G4 | 250 | 8 | 32 | 4 | 4 | 6.9 | 20 |

TABLE II
CASES SETTINGS

| Case | Frequency security constraints | FR provided by BES | WTG under PRM | WTG under PURM |
|---|---|---|---|---|
| 1 | × | × | × | × |
| 2.1 | √ | × | × | × |
| 2.2 | √ | × | × | √ |
| 2.3 | √ | × | √ | × |
| 2.4 | √ | × | √ | √ |
| 3.1 | √ | √ | × | × |
| 3.2 | √ | √ | × | √ |
| 3.3 | √ | √ | √ | × |
| 3.4 | √ | √ | √ | √ |

## B. Results

The economic results of the above cases and their frequency response indices under the most serious scheduling period are shown in Table III. The operation cost of Case 1 is the lowest (2245.96 k$), and the power from RE can be fully consumed. However, the maximum ROCOF, frequency nadir, and steady-state frequency after contingency are 0.6227 Hz/s, 49.08 Hz, and 49.55 Hz, respectively, which violate the constraints.

TABLE III
ECONOMIC RESULTS AND FREQUENCY RESPONSE INDICES OF DIFFERENT CASES

| Case | Cost (k$) | Extra cost (%) | RE curtailment (%) | ROCOF (Hz/s) | $f_{nadir}$ (Hz) | $f_{ss}$ (Hz) |
|---|---|---|---|---|---|---|
| 1 | 2245.96 | 0 | 0 | 0.6227 | 49.08 | 49.55 |
| 2.1 | 2553.56 | 13.70 | 8.04 | 0.3401 | 49.41 | 49.74 |
| 2.2 | 2433.24 | 8.34 | 6.08 | 0.3121 | 49.40 | 49.72 |
| 2.3 | 2353.80 | 4.80 | 2.86 | 0.4000 | 49.40 | 49.71 |
| 2.4 | 2321.60 | 3.37 | 1.63 | 0.4000 | 49.40 | 49.70 |
| 3.1 | 2271.27 | 1.13 | 0.72 | 0.3798 | 49.40 | 49.70 |
| 3.2 | 2254.90 | 0.40 | 0.09 | 0.3213 | 49.40 | 49.70 |
| 3.3 | 2259.54 | 0.60 | 0.19 | 0.4000 | 49.40 | 49.70 |
| 3.4 | 2253.97 | 0.36 | 0.08 | 0.4000 | 49.40 | 49.70 |

*1) Effectiveness of Frequency Security Constraints in Scheduling*

Imposing frequency security constraints into the model, the frequency dynamic indices of the system satisfy the security constraints. Extra FR capabilities are needed so that the operation cost of the system will increase. In Case 2.1, the FR capabilities from WTG and BES are not included, and the system needs more SGs to ensure the frequency security. Due to the minimum technical output limit of SGs, RE cannot be fully consumed, and the RE curtailment rate is 8.04%. The operation cost of Case 2.1 is 2553.56 k$, which means that 13.70% of the extra cost is needed for frequency security.

*2) Effectiveness of Support from Multi-source Converters in Frequency-constrained Scheduling Model*

With further consideration of the FR capabilities from WTG and BES, the FR demand from SGs can be reduced. The starting capacity of SGs can be determined more flexibly to consume more power from RE, making the system more economical. When BES does not provide FR, if WTG participates in FR through the PURM (Case 2.2) or PRM (Case 2.3), the operation cost will be reduced to 2433.24 k$ and 2353.80 k$, respectively. In Case 2.4, where WTG can switch between the PRM and PURM flexibly according to the system status, the cost will further reduce to 2321.60 k$. Compared with FR provided by WTG under a single PRM or PURM, flexible switching between the PRM and PURM can make the system more economical. In the cases where the FR from BES is considered, the costs further drop to 2271.27 k$ (Case 3.1), 2254.90 k$ (Case 3.2), 2259.54 k$ (Case 3.3), and 2253.97 k$ (Case 3.4) with different FR modes from WTG, respectively. In the proposed Case 3.4, which coordinates FR capabilities from BES and WTG under both the PURM and PRM, frequency security constraints can be perfectly satisfied, sacrificing only 0.36% in extra cost compared with Case 1.

Compared with Case 2.1 where only the frequency support from the SGs is modeled, the consideration of support from multi-source converters (Case 3.4) reduces system costs from 2553.56 k$ to 2253.97 k$. The introduction of frequency support from multi-source converters reduces the

cost of the frequency-constrained scheduling model by 11.73%.

*3) Frequency Response Characteristics*

Figures 8 and 9 show the frequency dynamic indices after contingency during each scheduling period in the RE scenario with the highest probability. The case where frequency constraints are not considered (Case 1) will lead to insecurity after contingency, especially during 11:00-17:00 when the amount of available power from RE is large and several SGs are shut down. The proposed Case 3.4 can arrange for more SGs and other FR resources to be online to provide the required frequency support, making the system meet the frequency security constraints.

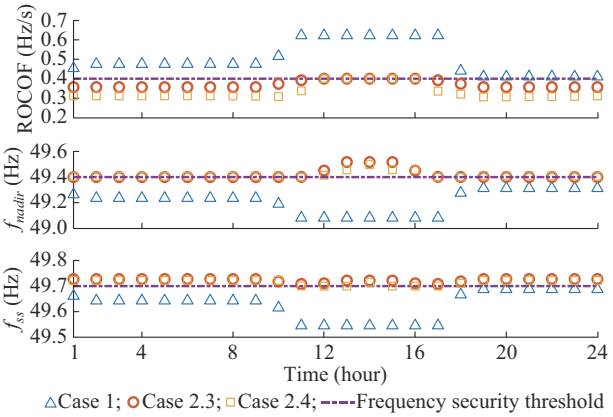


Fig. 8. Frequency dynamic characteristics of Case 2.3 and Case 2.4 compared with Case 1.

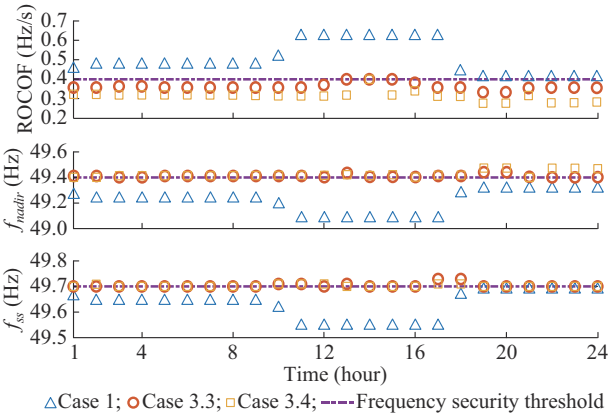


Fig. 9. Frequency dynamic characteristics of Case 3.3 and Case 3.4 compared with Case 1.

*4) Inertia Composition*

The inertia composition during each scheduling period of the system is shown in Fig. 10. After contingency, the ROCOF of the system is directly related to the comprehensive inertia $H^{SYS}$.

As shown in (56), if BES does not participate in FR (Case 1 and Cases 2.1-2.4), $H^{SYS}$ of the system shall not be less than 5 s to meet the ROCOF constraint, i.e.,

$$H^{SYS} \geq \frac{P_{IM} f_0}{2S_{sys} \left| ROCOF_{\max,set} \right|} = \frac{800 \times 50}{2 \times 10000 \times 0.4} = 5 \text{ s} \tag{56}$$

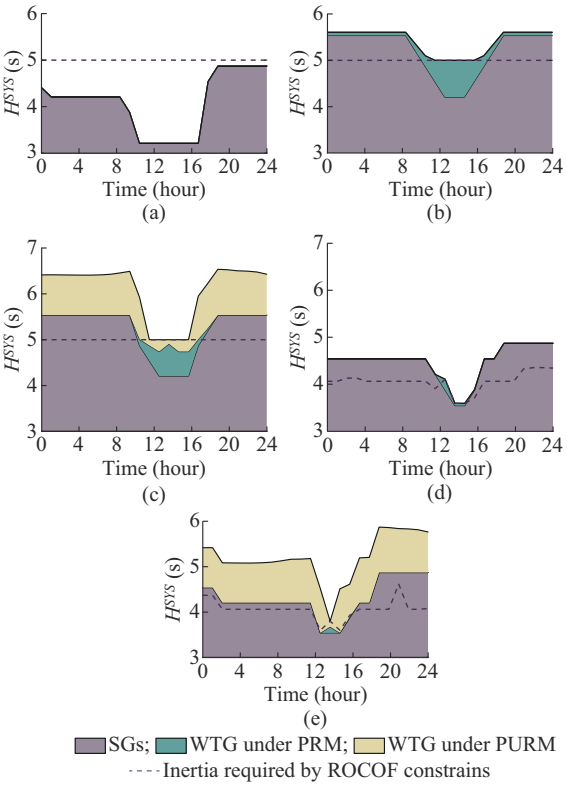


Fig. 10. Inertia composition during each scheduling period. (a) Case 1. (b) Case 2.3. (c) Case 2.4. (d) Case 3.3. (e) Case 3.4.

In Case 1, WTG and BES do not participate in FR, and the inertia provided by SGs of the system cannot meet the ROCOF constraints. There is no wind power curtailment in Case 1. The reserved wind power needed for FR is shown in Fig. 11. In Case 2.3, WTG provides virtual inertia for the system through the PRM to ensure sufficient frequency inertia in the system. However, this will lead to a large amount of wind curtailment, which will conspicuously reduce the economy of the system. In Case 2.4, WTG can provide certain virtual inertia through the PRUM to reduce the required reserved power of WTG under the PRM and save the operation cost of the system to a certain extent.

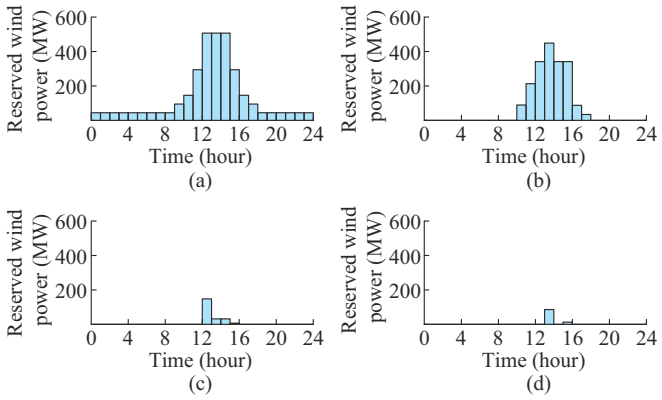


Fig. 11. Reserved wind power needed for FR. (a) Case 2.3. (b) Case 2.4. (c) Case 3.3. (d) Case 3.4.

In Case 3.3 and Case 3.4, the BES can increase its output power instantaneously as soon as contingency occurs to re-

duce the imbalanced power. The required comprehensive inertia of the system to meet the ROCOF constraints is reduced, and the demand for reserved wind power decreases.

### C. Discussion

#### 1) Accuracy of Linearization Constraints for Frequency Nadir

Figure 12 shows the effects of the proposed method for improving the approximation accuracy of the linearized frequency nadir constraints in Case 3.4. Note that focus on the accuracy of frequency nadir constraints, ROCOF constraints and steady-state frequency constraints are removed here. So that the accuracy of frequency nadir constraints is focused on. As shown in Table IV, compared with the original linearization method where the domain of definition of $\chi$ is set to a fixed value in advance, the improved linearization method can adaptively cut the domain of definition of $\chi$ and improve the approximation accuracy. The linearized frequency nadir constraints of the original linearization method limit the frequency nadir to above 49.4084 Hz in the scheduling model, which is 0.0084 Hz higher than the setting (49.4000 Hz). The improved linearization method reduces the linearization error to 0.0007 Hz and lowers the operation cost from 2251.41 k$ to 2250.01 k$.

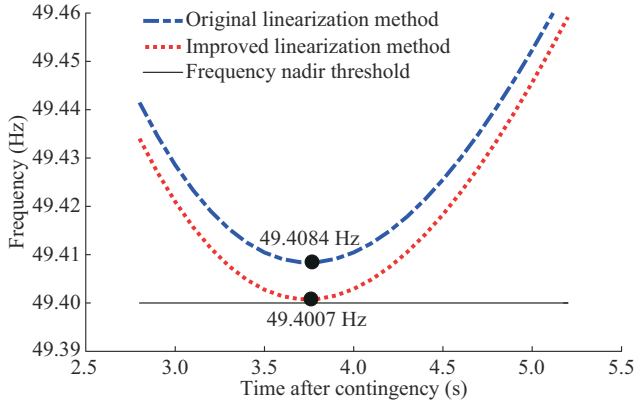


Fig. 12. Effects of proposed method for improving approximation accuracy of linearized frequency nadir constraints.

TABLE IV
COMPARISON OF ORIGINAL AND IMPROVED LINEARIZATION METHODS

| Linearization method | Cost (k$) | $f_{nadir}$ (Hz) | Frequency nadir error of linearization (Hz) |
|---|---|---|---|
| Original | 2251.41 | 49.4084 | 0.0084 |
| Improved | 2250.01 | 49.4007 | 0.0007 |

#### 2) Impacts of Installed BES Power on Economic Results

Figure 13 shows the impacts of installed BES power on the operation cost in Cases 1, 2.4, and 3.4. The increment of installed BES power has a very small impact on the reduction of operation cost in Case 1 where frequency security constraints are not considered and Case 2.4 where BES does not provide FR. In Case 3.4 where FR capabilities from the BES are modeled, the operation cost of the system decreases significantly with increasing installed BES power. This shows that participating in emergency frequency support can effectively improve the marginal revenue of BES construction in the frequency-constrained scheduling model.

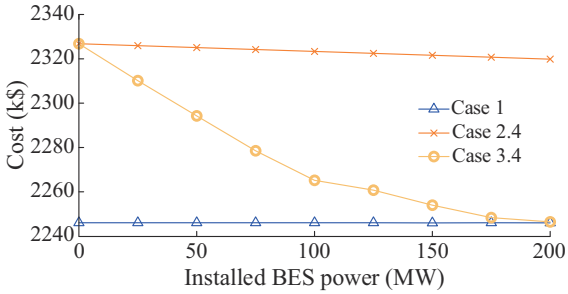


Fig. 13. Total operation costs in Cases 1, 2.4, and 3.4 with different installed BES power.

#### 3) Impacts of Wind Penetration on Economic Results

The cost increments of Cases 2.3, 2.4, 3.3, and 3.4 compared with Case 1 under different wind power penetrations are shown in Fig. 14. When the proportion of wind power is less than 40%, Cases 3.3 and 3.4 have the same operation cost as Case 1, which means that frequency security constraints do not bring additional cost. With the rise of wind power penetration, the operation cost increment caused by frequency security constraints becomes more obvious. The proposed Case 3.4 can guarantee frequency security within less than 4% of the extra cost in a system with a wind power penetration of 60%.

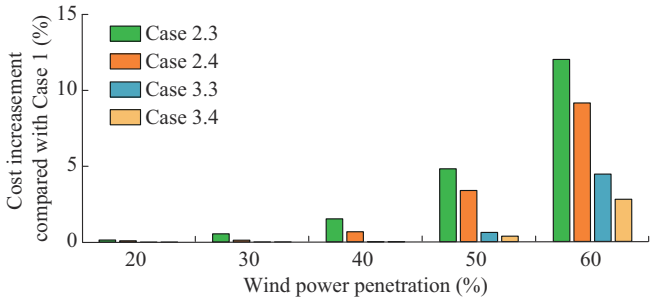


Fig. 14. Cost increment compared with Case 1 under different wind power penetrations.

## VI. CONCLUSION

Frequency support from multi-source converters is necessary to maintain frequency security in power systems with high RE penetration. FR performance is related to the working states, operation modes, and parameters of the converters, and it is essential to coordinate these variable factors. In this paper, we establish an integrated frequency-constrained scheduling model considering the coordination of variable FR capabilities from multi-source converters. The operation states and FR capabilities of converter-based WTG and BES are modeled and integrated into the frequency dynamic functions. By linearizing frequency security constraints, the scheduling model is converted to a standard MILP problem.

Numerical results validate the effectiveness of the proposed methods and indicate the three following points.

1) The system can ensure frequency security at the lowest additional cost by coordinating the operation state and FR parameters of WTG and BES. The consideration of frequen-

cy support from multi-source converters reduces the cost of the frequency-constrained scheduling model by 11.73%.

2) Flexible adjustment of FR parameters and strategies can guarantee sufficient FR capabilities during each scheduling period so that the frequency dynamic will not violate the security boundaries under contingency.

3) Frequency security constraints become more difficult to meet with an increasing proportion of WTG. The proposed method can ensure frequency security within less than 4% extra cost for a test system with WTG penetration of 60%.

As frequency support can be conducted between the power grids connected through voltage source converter based HVDC (VSC-HVDC), the coordinated FR capabilities with VSC stations require attention in future studies. Future works should consider the frequency support of grid-forming converters. In addition, as frequency dynamics often accompany voltage fluctuations, the management of reactive power and voltage in a stability-constrained scheduling model deserves further attention.

## REFERENCES


[1] H. I. Jager, R. A. Efroymson, and R. A. McManamay, "Renewable energy and biological conservation in a changing world," *Biological Conservation*, vol. 263, p. 109354, Nov. 2021.

[2] P. Veers, K. Dykes, E. Lantz *et al.*, "Grand challenges in the science of wind energy," *Science*, vol. 366, no. 6464, pp. 1-11, Oct. 2019.

[3] S. Homan, N. M. Dowell, and S. Brown, "Grid frequency volatility in future low inertia scenarios: challenges and mitigation options," *Applied Energy*, vol. 290, p. 116723, May 2021.

[4] D. Sun, X. Han, B. Zhang *et al.*, "Frequency aware robust economic dispatch," *Journal of Modern Power Systems and Clean Energy*, vol. 4, no. 2, pp. 200-210, Apr. 2016.

[5] S. Banik, M. S. Sakib, S. Chowdhury *et al.*, "Inertia constrained economic dispatch in a renewable dominated power system," in *Proceedings of 2021 IEEE PES Innovative Smart Grid Technologies Conference – Latin America (ISGT Latin America)*, Lima, Peru, Sept. 2021, pp. 1-5.

[6] S. Pöschel-Løvengreen and P. Mancarella, "Frequency response constrained economic dispatch with consideration of generation contingency size," in *Proceedings of 2018 Power Systems Computation Conference (PSCC)*, Dublin, Ireland, Jun. 2018, pp. 1-7.

[7] Y. Lee and R. Baldick, "A frequency-constrained stochastic economic dispatch model," *IEEE Transactions on Power Systems*, vol. 28, no. 3, pp. 2301-2312, Aug. 2013.

[8] F. Teng, V. Trovato, and G. Strbac, "Stochastic scheduling with inertia-dependent fast frequency response requirements," *IEEE Transactions on Power Systems*, vol. 31, no. 2, pp. 1557-1566, Mar. 2016.

[9] C. Cardozo, L. Capely, and P. Dessante, "Frequency constrained unit commitment," *Energy Systems*, vol. 8, no. 1, pp. 31-56, Feb. 2017.

[10] A. B. T. Attya and J. L. Dominguez-García, "Insights on the provision of frequency support by wind power and the impact on energy systems," *IEEE Transactions on Sustainable Energy*, vol. 9, no. 2, pp. 719-728, Apr. 2018.

[11] T. Xu, W. Jang, and T. Overbye, "Commitment of fast-responding storage devices to mimic inertia for the enhancement of primary frequency response," *IEEE Transactions on Power Systems*, vol. 33, no. 2, pp. 1219-1230, Mar. 2018.

[12] F. Teng and G. Strbac, "Assessment of the role and value of frequency response support from wind plants," *IEEE Transactions on Sustainable Energy*, vol. 7, no. 2, pp. 586-595, Apr. 2016.

[13] V. Prakash, P. Kushwaha, K. C. Sharma *et al.*, "Frequency response support assessment from uncertain wind generation," *International Journal of Electrical Power & Energy Systems*, vol. 134, p. 107465, Jan. 2022.

[14] F. Zhang, Z. Hu, X. Xie *et al.*, "Assessment of the effectiveness of energy storage resources in the frequency regulation of a single-area power system," *IEEE Transactions on Power Systems*, vol. 32, no. 5, pp. 3373-3380, Sept. 2017.

[15] L. Meng, J. Zafar, S. K. Khadem *et al.*, "Fast frequency response from energy storage systems – a review of grid standards, projects and technical issues," *IEEE Transactions on Smart Grid*, vol. 11, no. 2, pp. 1566-1581, Mar. 2020.

[16] J. F. Restrepo and F. D. Galiana, "Unit commitment with primary frequency regulation constraints," *IEEE Transactions on Power Systems*, vol. 20, no. 4, pp. 1836-1842, Nov. 2005.

[17] X. Lei, E. Lerch, and C. Xie, "Frequency security constrained short-term unit commitment," *Electric Power Systems Research*, vol. 60, no. 3, pp. 193-200, Jan. 2002.

[18] L. Hao, J. Ji, D. Xie *et al.*, "Scenario-based unit commitment optimization for power system with large-scale wind power participating in primary frequency regulation," *Journal of Modern Power Systems and Clean Energy*, vol. 8, no. 6, pp. 1259-1267, Nov. 2020.

[19] A. Safari and H. Shahsavari, "Frequency-constrained unit commitment problem with considering dynamic ramp rate limits in the presence of wind power generation," *Neural Computing and Applications*, vol. 31, no. 9, pp. 5241-5254, Sept. 2019.

[20] Y. Zhang, H. Cui, J. Liu *et al.*, "Encoding frequency constraints in preventive unit commitment using deep learning with region-of-interest active sampling," *IEEE Transactions on Power Systems*, vol. 37, no. 3, pp. 1942-1955, May 2022.

[21] H. Ahmadi and H. Ghasemi, "Security-constrained unit commitment with linearized system frequency limit constraints," *IEEE Transactions on Power Systems*, vol. 29, no. 4, pp. 1536-1545, Jul. 2014.

[22] M. Farrokhabadi, C. A. Cañizares, and K. Bhattacharya, "Unit commitment for isolated microgrids considering frequency control," *IEEE Transactions on Smart Grid*, vol. 9, no. 4, pp. 3270-3280, Jul. 2018.

[23] M. Javadi, T. Amraee, and F. Capitanescu, "Look ahead dynamic security-constrained economic dispatch considering frequency stability and smart loads," *International Journal of Electrical Power & Energy Systems*, vol. 108, pp. 240-251, Jun. 2019.

[24] S. Jiang, C. Wu, S. Gao *et al.*, "Coordinative frequency-constrained unit commitment model for HVDC interconnected AC systems," *International Journal of Electrical Power & Energy Systems*, vol. 141, p. 108176, Oct. 2022.

[25] L. Badesa, F. Teng, and G. Strbac, "Simultaneous scheduling of multiple frequency services in stochastic unit commitment," *IEEE Transactions on Power Systems*, vol. 34, no. 5, pp. 3858-3868, Sept. 2019.

[26] M. Paturet, U. Markovic, S. Delikaraoglou *et al.*, "Stochastic unit commitment in low-inertia grids," *IEEE Transactions on Power Systems*, vol. 35, no. 5, pp. 3448-3458, Sept. 2020.

[27] Z. Zhang, E. Du, F. Teng *et al.*, "Modeling frequency dynamics in unit commitment with a high share of renewable energy," *IEEE Transactions on Power Systems*, vol. 35, no. 6, pp. 4383-4395, Nov. 2020.

[28] Z. Zhang, E. Du, G. Zhu *et al.*, "Modeling frequency response dynamics in power system scheduling," *Electric Power Systems Research*, vol. 189, p. 106549, Dec. 2020.

[29] C. J. Ferrandon-Cervantes, B. Kazemtabrizi, and M. C. M. Troffaes, "Inclusion of frequency stability constraints in unit commitment using separable programming," *Electric Power Systems Research*, vol. 203, p. 107669, Feb. 2022.

[30] Z. Chu, U. Markovic, G. Hug *et al.*, "Towards optimal system scheduling with synthetic inertia provision from wind turbines," *IEEE Transactions on Power Systems*, vol. 35, no. 5, pp. 4056-4066, Sept. 2020.

[31] Y. Yuan, Y. Zhang, J. Wang *et al.*, "Enhanced frequency-constrained unit commitment considering variable-droop frequency control from converter-based generator," *IEEE Transactions on Power Systems*, vol. 38, no. 2, pp. 1094-1110, Mar. 2023.

[32] J. Luo, F. Teng, S. Bu *et al.*, "Converter-driven stability constrained unit commitment considering dynamic interactions of wind generation," *International Journal of Electrical Power & Energy Systems*, vol. 144, p. 108614, Jan. 2023.

[33] Z. Zhang, M. Zhou, Z. Wu *et al.*, "A frequency security constrained scheduling approach considering wind farm providing frequency support and reserve," *IEEE Transactions on Sustainable Energy*, vol. 13, no. 2, pp. 1086-1100, Apr. 2022.

[34] H. Li, Y. Qiao, Z. Lu *et al.*, "Frequency-constrained stochastic planning towards a high renewable target considering frequency response support from wind power," *IEEE Transactions on Power Systems*, vol. 36, no. 5, pp. 4632-4644, Sept. 2021.

[35] Y. Wen, W. Li, G. Huang *et al.*, "Frequency dynamics constrained unit commitment with battery energy storage," *IEEE Transactions on Power Systems*, vol. 31, no. 6, pp. 5115-5125, Nov. 2016.

[36] S. Yan, Y. Zheng, and D. J. Hill, "Frequency constrained optimal siting and sizing of energy storage," *IEEE Access*, vol. 7, pp. 91785-91798, Jul. 2019.

[37] V. Trovato, A. Bialecki, and A. Dallagi, "Unit commitment with inertia-dependent and multispeed allocation of frequency response servic-

es," *IEEE Transactions on Power Systems*, vol. 34, no. 2, pp. 1537-1548, Mar. 2019.
[38] S. S. Oskouee, S. Kamali, and T. Amraee, "Primary frequency support in unit commitment using a multi-area frequency model with flywheel energy storage," *IEEE Transactions on Power Systems*, vol. 36, no. 6, pp. 5105-5119, Nov. 2021.
[39] V. Knap, S. K. Chaudhary, D.-I. Stroe *et al.*, "Sizing of an energy storage system for grid inertial response and primary frequency reserve," *IEEE Transactions on Power Systems*, vol. 31, no. 5, pp. 3447-3456, Sept. 2016.
[40] Y. Ye, Y. Qiao, and Z. Lu, "Revolution of frequency regulation in the converter-dominated power system," *Renewable & Sustainable Energy Reviews*, vol. 111, pp. 145-156, Sept. 2019.
[41] X. Zhao, Z. Lin, B. Fu *et al.*, "Research on frequency control method for micro-grid with a hybrid approach of FFR-OPPT and pitch angle of wind turbine," *International Journal of Electrical Power & Energy Systems*, vol. 127, p. 106670, May 2021.
[42] A. B. Attya, J. L. Dominguez-Garcia, and O. Anaya-Lara, "A review on frequency support provision by wind power plants: current and future challenges," *Renewable & Sustainable Energy Reviews*, vol. 81, pp. 2071-2087, Jan. 2018.
[43] Z. Wu, W. Gao, T. Gao *et al.*, "State-of-the-art review on frequency response of wind power plants in power systems," *Journal of Modern Power Systems and Clean Energy*, vol. 6, no. 1, pp. 1-16, Jan. 2018.
[44] M. Sun, Y. Min, X. Xiong *et al.*, "Practical realization of optimal auxiliary frequency control strategy of wind turbine generator," *Journal of Modern Power Systems and Clean Energy*, vol. 10, no. 3, pp. 617-626, May 2022.
[45] Z. Lu, Y. Ye, and Y. Qiao, "An adaptive frequency regulation method with grid-friendly restoration for VSC-HVDC integrated offshore wind farms," *IEEE Transactions on Power Systems*, vol. 34, no. 5, pp. 3582-3593, Sept. 2019.
[46] A. Khan, M. Seyedmahmoudian, A. Raza *et al.*, "Analytical review on common and state-of-the-art FR strategies for VSC-MTDC integrated offshore wind power plants," *Renewable & Sustainable Energy Reviews*, vol. 148, p. 111106, Sept. 2021.
[47] U. Akram, M. Nadarajah, R. Shah *et al.*, "A review on rapid responsive energy storage technologies for frequency regulation in modern power systems," *Renewable & Sustainable Energy Reviews*, vol. 120, p. 109626, Mar. 2020.
[48] Y. Yoo, S. Jung, and G. Jang, "Dynamic inertia response support by energy storage system with renewable energy integration substation," *Journal of Modern Power Systems and Clean Energy*, vol. 8, no. 2, pp. 260-266, Mar. 2020.
[49] K. Wang, Y. Qiao, L. Xie *et al.*, "A fuzzy hierarchical strategy for improving frequency regulation of battery energy storage system," *Journal of Modern Power Systems and Clean Energy*, vol. 9, no. 4, pp. 689-698, Jul. 2021.
[50] Y. Jiang, E. Cohn, P. Vorobev *et al.*, "Storage-based frequency shaping control," *IEEE Transactions on Power Systems*, vol. 36, no. 6, pp. 5006-5019, Nov. 2021.
[51] L. Miao, J. Wen, H. Xie *et al.*, "Coordinated control strategy of wind turbine generator and energy storage equipment for frequency support," *IEEE Transactions on Industry Applications*, vol. 51, no. 4, pp. 2732-2742, Jul./Aug. 2015.
[52] S. Zhang, Y. Mishra, and M. Shahidehpour, "Fuzzy-logic based frequency controller for wind farms augmented with energy storage systems," *IEEE Transactions on Power Systems*, vol. 31, no. 2, pp. 1595-1603, Mar. 2016.
[53] A. Junyent-Ferr, Y. Pipelzadeh, and T. C. Green, "Blending HVDC-link energy storage and offshore wind turbine inertia for fast frequency response," *IEEE Transactions on Sustainable Energy*, vol. 6, no. 3, pp. 1059-1066, Jul. 2015.
[54] J. Liu, J. Wen, Y. Long *et al.*, "Solution to short-term frequency response of wind farms by using energy storage systems," *IET Renewable Power Generation*, vol. 10, no. 5, pp. 669-678, May 2016.
[55] J. Lee, E. Muljadi, P. Srensen *et al.*, "Releasable kinetic energy-based inertial control of a DFIG wind power plant," *IEEE Transactions on Sustainable Energy*, vol. 7, no. 1, pp. 279-288, Jan. 2016.
[56] Y. Tan, L. Meegahapola, and K. M. Muttaqi, "A suboptimal power-point-tracking-based primary frequency response strategy for DFIGs in hybrid remote area power supply systems," *IEEE Transactions on Energy Conversion*, vol. 31, no. 1, pp. 93-105, Mar. 2016.
[57] Y. Zhang, J. Wang, T. Ding *et al.*, "Conditional value at risk-based stochastic unit commitment considering the uncertainty of wind power generation," *IET Generation, Transmission & Distribution*, vol. 12, no. 2, pp. 482-489, Jan. 2018.

**Jiaming Li** received the B.S. degree in electrical engineering from the Department of Electrical Engineering, Tsinghua University, Beijing, China, in 2019, where he is currently pursuing the Ph.D. degree in electrical engineering. His research interests include power system frequency security and the application of artificial intelligence and big data technology in power systems.

**Ying Qiao** received the B.S. and Ph.D. degrees in electrical engineering from Shanghai Jiao Tong University, Shanghai, China, and Tsinghua University, Beijing, China, in 2002 and 2008, respectively. Since 2010, she has been with Tsinghua University, where she is currently an Associate Professor of Electrical Engineering. Her research interests include renewable energy and power system security and control.

**Zongxiang Lu** received the B.S. and Ph.D. degrees in electrical engineering from Tsinghua University, Beijing, China, in 1998 and 2002, respectively. Since 2002, he has been with Tsinghua University, where he is currently an Associate Professor. His research interests include large-scale wind power/photovoltaic (PV) stations integration analysis and control, energy and electricity strategy planning, power system reliability, distributed grid (DG), and microgrid.

**Wei Ma** received the B.S. degree in automation from Xinjiang University, Urumqi, China, in 2020. Currently, he is pursuing the M.S. degree in control science and engineering from Xinjiang University. He is currently participating in joint research with Tsinghua University, Beijing, China. His research interests include wind power forecasting and power system scheduling.

**Xin Cao** received the B.S. degree from Huazhong University of Science and Technology, Wuhan, China, in 1992, and the M.S. and Ph.D. degrees from Renmin University of China, Beijing, China, in 1999 and 2003, respectively. He is currently the Chairman of the Board with China Suntien Green Energy Co., Ltd, Shijiazhuang, China. His research interests include power system operation and control, and optimized operation of integrated energy system.

**Rongfu Sun** received the B.S. degree from the Shanghai University of Electric Power, Shanghai, China, in 2002, the M.S. degree from Wuhan University, Wuhan, China, in 2005, and the Ph.D. degree from Tsinghua University, Beijing, China, in 2009, all in electrical engineering. He is currently a Power Market Manager with Jibei Electric Power Company, Beijing, China. His research interests include renewable energy forecasting and generation scheduling, and active power coordinated control.